Science and Technology Publishing (SCI & TECH)
ISSN: 2632-1017
Vol. 5 Issue 3, March - 2021

Modeling, Characterization And Optimization Of Solar Tracker Using Proportional Integral (PI) Controller

Oduobuk, Enobong Joseph
Department of Physics
University of Uyo
enobong_joseph1@yahoo.com

Obianwu, Victor Ifanyi
Department of Physics
University of Calabar
vimoseis@yahoo.co.uk

Akpabio, Idara Okon
Department of Physics
University of Uyo
idaraakpabio@uniuyo.edu.ng

Abstract*— In this research work, modeling, characterization and optimization of a solar tracker using proportion and integral (PI) controller was carried out, to regulate the tracking process so that optimum energy is derived from the PV cell throughout the day time. The solar tracker control system is modeled and designed using MATLAB software. Materials and components used include direct current (dc) motor system, proportional and integral (PI) controller and photovoltaic cell (PV). A mathematical approach was used to develop and model the sub-systems and the overall cascade system transfer function equations, which include the inner and outer proportional integral (PI) controller loop transfer function, dynamic model of dc motor (electrical and mechanical) armature - controlled transfer function and photovoltaic cell domain equation transfer function. The Simulink models of open and closed loop transfer functions of the sub-system and main process systems were also developed, simulated and analyzed, from where the performance and stability indices of the system are derived. They include simulink open loop dc motor internal structure model, dc motor subsystem model, photovoltaic internal structure model, photovoltaic subsystem model and the overall cascade model. Others include closed loop simulink with proportional gain on dc motor system, dc motor subsystem with proportional integral controller and photovoltaic cell with proportional integral controller. Results of simulation yielded a relatively low in rise time, settling time and steady state error of 0.4 second, 1.8 second and 0.0 rad/s. The results also showed that coupling proportional integral controller with photovoltaic cell reduces rise and settling time to a relatively low value of 1.6 seconds and 5.5 seconds respectively. Hence, using a proportional integral controller on solar tracking has reduced the rise time performance index by 77.8% and caused system stability to decrease to 67.2%, as compared to the existing system. The results imply that with proportional integral controller, it takes a shorter time for the solar tracker to respond to sudden change in input signal and quickly positions the photovoltaic cell at desired angle. The shorter time and speed achieved in this system means that only smaller amount of power would be required to position the PV cell appropriately. Therefore, using proportional integral (PI) controller in solar tracking system has improved the tracking performance and stability in terms of desired position, speed and time response. Thus, PI controller is highly recommended for solar energy tracking because it is capable of reducing the system rise time, settling time and eliminate overshoot, undershoot, steady state error..

Keywords*— Simulink, Model, Photovoltaic, System, Controller, Open Loop, Closed Loop

I. INTRODUCTION

In this modern world, the most important element which drives the essential needs of life is the use of electric energy. This electric energy is gotten from two major sources, it is either a renewable or non-renewable source (Islam *et al.,* 2014). There are four major renewable energy sources which are wind energy, hydro energy, geothermal energy and solar energy. The non-renewable energy resources such as coal, nuclear, oil, and natural gas, but there are available in limited supplies. However, the threat posed by most non-renewable energy sources such as global warming and future sustainability has led to the growing need of renewable energy in the world today. Therefore, this has also prompt further researches to be carried out especially in the area of wind power, solar power and hydro power. Although other renewable sources may show a promising result in the nearest future, but one tends to find out a more proficient method of harvesting, optimizing and expanding the use of solar energy at it threshold.

The sun is a major source of inexhaustible free energy for the planet earth and nearly all the existing energy sources is as a function of the sun (Wendy, 2009); (Deb and Roy, 2012). It is observed that the power from the sun intercepted by the earth is approximately $1.8\,X\,10^{11}$ MW (Bala and Rajesh, 2014). This is seen as enormous energy for the world today and the future, but the effective method of harvesting and converting solar energy to electricity is seen as challenge. However, solar energy is broadly classified in two categories on the basis of usage, which is active and passive method. In other words, solar energy from the sun can be harnessed into two major ways; electricity and thermal (Genesis, 2010). In solar electricity system, which photovoltaic (PV) cell panel, it is used to converts solar radiation (photons) into electricity. While solar thermal method is the use of solar thermal collectors to harvest sun energy, which involves heat collection from sunlight as direct application (Genesis, 2010). But among the two methods of harvesting solar energy, it is only the

conversion of solar radiation into electricity through the use of PV cell that is mostly adopted.

Basically, most static solar panels generate little or low output due to the sun's movement in the day time. This unstable source of solar radiation due to the rotation of the Earth has course most static solar panel systems to become under-utilized, hence recording relatively low output efficiency. Also, the output voltage of the PV module reduces as module temperature increases, and most solar tracker designs are voltage based when the PV cell output current is unaffected by increase in temperature. So this is taken into consideration in this research work.

Moreover, when mounting PV modules on the roof, the PV module heat up substantially as inner temperatures increases from 50 – 75 ^{0}C. So this is a problem of poor ventilation and this is a challenge as it reduces the photovoltaic cell efficiency. Also, the continuous use of bulky and numerous components as captured in most research work to build solar tracking systems is seen as a problem. It therefore means that a huge percentage of the power tracked or harvested from the sun is almost used up during the tracking process, so this is a grey area which must be addressed. Therefore, this problem faced by this research is to find a way and possibly formulate appropriate models and methods of fully harnessing maximally the energy from the sun. The solution involve designing and developing models, including dynamic system of solar tracker using proportional and integral (PI) controllers, to control and, position solar panel (PV cell) and possibly, enhance cooling and optimize the solar tracking capabilities in terms of speed and accuracy.

II. RELATED WORK

Solar energy is gradually gaining global attention due to the growing need of clean and sustainable power supply, many have carried out researches using different methods and approaches which yield some results but also create research gaps. For instant

Bamigboye *et al.* (2016), developed a solar tracking system using internal model control (IMC-PID) controller. PID controller was used coupled with Internal Model Control (IMC), Chien-Hrones-Reswick (CHR), Zeigler Nichol (ZN) and Tyreus-Luyben (TL**)** method**.** But the research gap showed that the system slowest rise and settling time, the present of sensor and D controller component makes system complex and bulky.

Kiyak and Gokhan (2016), did a comparison of fuzzy logic and PID controller for a single-axis solar tracking system. A result showed that the system has only one dimension of rotation, voltage based tracker and complex. Kumar and Sharma (2016), researched on improving performance of PV system using PID controller. But the approach lack system operation analysis (rise and settling time), it is a one dimensional system, voltage based tracker and appear to be complex in practice. Kalanithi and Rajesh (2014), developed an MPPT controller based solar tracking system. The system used a complex method which leads to bulky system and voltage based tracker. Baranwal and Dwivedi (2014), developed a solar tracking system that has a fixed solar panel which maintains constant maximum power output. The work lack frequency and time analysis, it is complex and bulky system. Ozerdem and Shahin (2014), developed a PV solar tracking system controlled by arduino/matlab/simulink. The system is a voltage based tracker system, it lacks operational concept (frequency and time analysis) and it is complex in practice. Balabel *et al.* (2013), worked on the design and performance of solar tracking photo-voltaic system. In the work, it employ voltage sensor which make the system complex with low accuracy and performance.

III. METHODOLOGY

The methodology employed in this research work involves control system design, development of control system model and control analysis. More details in modeling of system equations for inner and outer loop system controllers; proportional and integral (PI) controller loop transfer function, modeling of dc motor, dynamic model of armature controlled dc motor transfer function for would be analyzed. The mathematical modeling in electrical and mechanical domain, solar panel (photovoltaic cell); photovoltaic cell (solar panel) is also analyzed and expressed in terms of their transfer functions. Various system and subsystem SIMULINK are modeled in terms of open loop and closed loop transfer function. Also, the main process systems units is developed and simulated using MATLAB software and results obtained is analyzed for possible conclusion and recommendations.

(a) System Modeling and Analysis

In this aspect, all the sub-system and main system component employed in this work are modeled and analyzed. They include system design, mathematical models, transfer function of sub-systems, and Simulink models. However, let's consider system design by decoupling and analyzing the diagram in Figure 1.0.

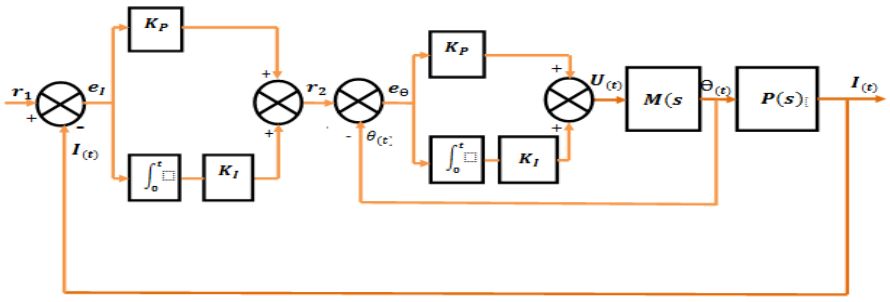

Figure1.0: Cascade control system block diagram of solar tracker

(i) Proportional Integral (PI) Controller Loop Transfer function

Lets consider the cascade control system block diagram in Figure 1.0. We have that:

$$U\ (t)\ \ = K_p e_\theta(t) + K_i \int_0^t e_\theta\ (t)\ dt \quad (1)$$

Taking Laplace transform of equation 1.0

L $[U\ (t)\ \ ]$ = L $[K_p e_\theta(t) + K_i \int_0^t e_\theta(t)\ dt]$

U (s) = $K_p E_\theta(s) + K_I \frac{1}{S} E_\theta(s)$

$$\boldsymbol{T.F_{PI}} = \frac{\boldsymbol{U(s)}}{\boldsymbol{E_\theta(s)}} = \frac{\boldsymbol{K_p S + K_I}}{\boldsymbol{S}} \quad (2)$$

(ii) Transfer Function of Dynamic Model of Armature Controlled DC Motor

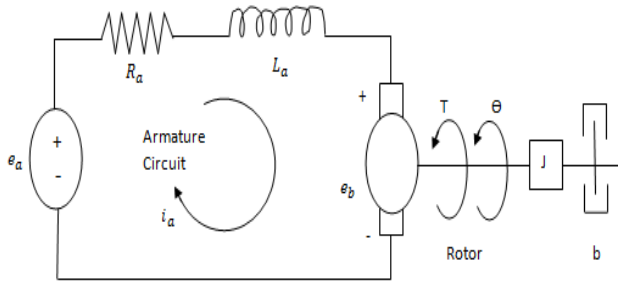

Figure 2: Equivalent circuit diagram of DC motor

(b) Model Parameters and Assumptions

Let b = Friction or damping coefficient of the mechanical part of the rotor.

J = Rotational inertia of the rotor.

K = Motor torque or Position of the coils with respect to the magnetic field (Constant)

$\vec{B}$ = Magnetic field constant

e_b = Back e.m.f induced in opposite direction due to the moving coil in the magnetic field.

K_b = Back e.m.f Constant.

T = Torque produce by the motor rotor

From Lorentz's (Thess, Votyakov, Knaepen and Zikanov, 2007) law we have;

$$\vec{F} = \vec{i_a} \times \vec{B} \quad (3)$$

$$\vec{T} = K_1 B i_a \quad (4)$$

Where K_1 is a constant signifying the position of the coil relative to the magnetic field.

But since it is armature control, it means the K and B are constant. Therefore, equation (4) becomes

$$T = K i_a \quad (5)$$

From Faraday's Law, the back e.m.f induced in opposite direction is given as;

$$e_b = K_b \frac{d\theta}{dt} \quad (6)$$

Where K_b = Back e.m.f constant.

(a) Electrical Domain Equation

To derive an equation describing the electrical dynamic of dc motor, we apply Kirchhoff voltage law (KVL) to the modeled circuit in Figure 2 and we have

$$e_a - R_a i_a - L_a \frac{di}{dt} - e_b = 0 \quad (7)$$

(b) Mechanical Domain Equation

Also, in mechanical domain, we apply Euler's law (Sparavigna, 2015) the equation becomes

$$T - b\dot{\theta} = J\ddot{\theta} \quad (8)$$

Where : $\dot{\theta}$ is speed of the motor

$\ddot{\theta}$ is the Angular Acceleration (rad/sec)

T - b$\dot{\theta}$ is the sum of the Moment.

In this case, before the electrical domain is coupled to mechanical domain, we first realize that the back e.m.f depends on the speed of the rotor while the torque is a function of the electric current, then we classified our output as position in terms of angle ($\theta_{(s)}$) and $E_{(s)}$ as input component.

However, since the transfer function of the dc motor is expressed;

$$T.F = \frac{Position}{Volatge} = \frac{\Theta(s)}{E_a(s)} \quad (9)$$

Substituting equation (6) into (7) we have equation for electrical domain to be;

$$e_a - R_a i_a - L_a \frac{di}{dt} - K_b \dot{\theta} = 0 \quad (10)$$

In this case equation (10) describes the electrical dynamic of the dc motor used.

But substituting equation (6) into (7) we obtained the mechanical equation to be;

$$K i_a - b\dot{\theta} = J\ddot{\theta} \quad (11)$$

Taking the Laplace transform of the electrical and mechanical equation in equation 10 and 11,

$$\text{For electrical: } L\ (e_a - R_a i_a - L_a \frac{di_a}{dt} - K_b \dot{\theta} = 0) \quad (12)$$

$$E_a(s) - R_a I_a(s) - L_a S I_a(s) - K_b S\Theta(s) = 0 \quad (13)$$

For Mechanical: L $(K i_a - b\dot{\theta})$ = L$(J\ddot{\theta})$

$$K I_a(s) - bS\theta(s) \ \ = J\theta \quad (14)$$

Eliminating $I_a(s)$, equation 14 is transformed to;

$$I_a\ (s) = \frac{(JS^2 + bS)\theta(s)}{K} \quad (15)$$

Putting (15) into (14) and rearranging, we have

$$E_a(s) = [(R_a + SL_a)(JS + b)\frac{S}{K} + K_b S]\ \theta(s) \quad (16)$$

By transforming equation (16),

$$\text{Transfer Function (T.F)} = \frac{\theta(s)}{E_a(s)} = \frac{1}{\frac{S}{K}(R_a + SL_a)(JS+b) + Kbs]}$$

To obtain the polynomial, we multiply by $\frac{K}{K}$

$$\frac{\theta(s)}{E_a(s)} = \frac{S}{K}\left(\frac{1}{R_a} + SL_a\right)(JS + b) + Kbs] \text{ x } \frac{K}{K}$$

$$\textbf{T.F} = \frac{\boldsymbol{\theta(s)}}{\boldsymbol{E(s)}} = \frac{\boldsymbol{K}}{\boldsymbol{S[(R_a+SL_a)(J_s+b)+KK_b]}}\left(\frac{\boldsymbol{radian}}{\boldsymbol{V}}\right) \quad \textbf{(17)}$$

Equation (17) is the transfer function of dynamic model of armature controlled dc motor.

(iii) Photovoltaic Cell (solar panel) Transfer Function

It is important to model the output of photovoltaic cell in terms of current, since the magnitude of photon current is directly proportional to the irradiance (i.e $I_{ph} \approx I_{sc}$). While the output voltage (V_{oc}) tends to saturate at a given temperature. However, let's consider the circuit in Figure 3;

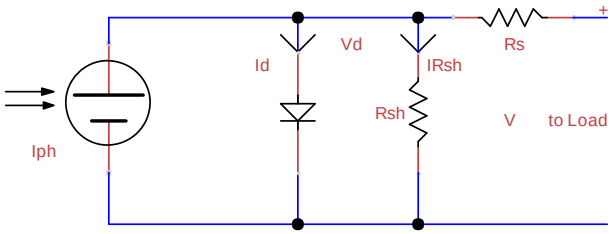

Figure 3: Equivalent circuit diagram of photovoltaic cell model

In Figure 3, the photovoltaic characterization include;

(a) The magnitude of the photo current depends on the following;
   i. Irradiance level
   ii. Light spectrum
   iii. Characteristics of the cell

(b) Short circuit current which is direct measure of the photon current (I_{Ph}) as specified at standard test condition (STC) are;
   - 1000W/m^2
   - Module temperature of 25^{0}C
   - Air mass (AM) = 1.5

(c) Magnitude of photon current (short circuit current) is directly proportional to the irradiance.

(iv) Diode Equation

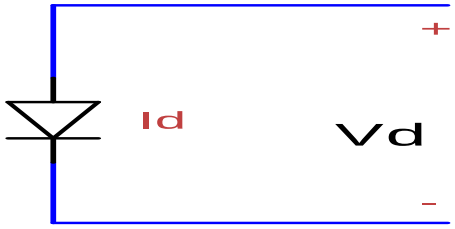

Figure 4: Circuit diagram of diode photovoltaic cell

According to Ankaiah and Nageswararao, (2013);

$$I_d = I_o[e^{\frac{qV_d}{aKT}} - 1] = I_o[e^{\frac{V_d}{V_{TH}}}] \quad (18)$$

Where T = Temperature in Kelvin (K)

q = Charge of an electron in coulombs (1.602 x 10^{-2} C)

K = Boltzmann constant (1.38 x 10^{-23} JK^{-1})

I_o = Dark or reverse saturation current of the diode at temperature (T).

a = Diode identification factor (normally between 1 & 2)

$V_{TH} = \frac{KT}{q}$ = Thermal voltage (V_{TH}) and is always 25.84mV for silicon at 300K at a = 1

R_{SH} = Shunt resistor (Ω)

R_s = Resistor in Series (Ω)

I_{Ph} = Photon current at a given irradiance and at temperature (T)

V_d = Voltage across the diode

(a) Series Resistance Equation

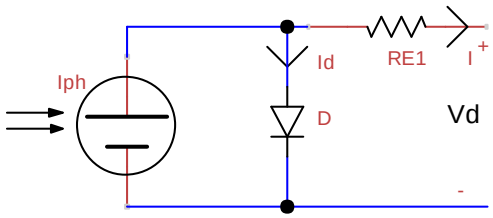

Figure 5: Circuit diagram of a series resistance configured photovoltaic cell

From Kirchhoff voltage law,

$$V_d = V + IR_s \quad (19)$$

$$I = I_{ph} - I_o(e^{\frac{q(V+IR_s)}{akT}} - 1) \quad (20)$$

(b) Shunt Resistance Equation

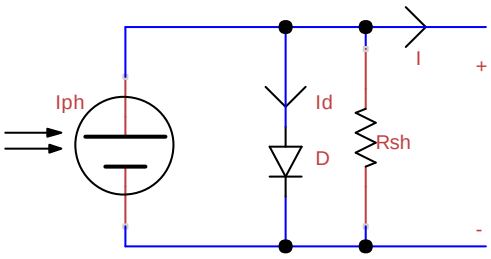

Figure 6: Circuit diagram of a shunt resistance configured photovoltaic cell

Recall that;

- R_{sh} models the leakage current of the p-n junction.
- Typical R_{sh} is a large volume, with low values representing defective cells
- Impact (on power loss) more pronounced at low irradiance levels.

For general PV cell equation, we Apply Kirchhoff Voltage (KVL) and current law (KI
L) to Figure 6 above, the total current (I) flowing in the circuit becomes;

$$I = I_{ph} - I_d - I_{sh} \quad (21)$$

$$\text{That is; } I = I_{Ph} - I_o[e^{\frac{V_d}{V_{th}}} - 1] - [\frac{V+IR_s}{R_{sh}}] \quad (22)$$

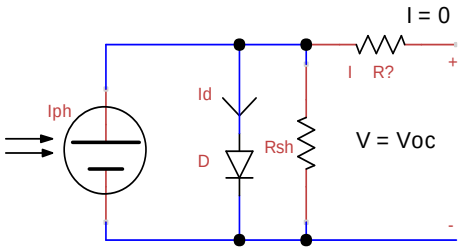

Figure 7: Circuit Diagram of a Complete Photovoltaic Cell Model

For a maximum possible voltage of PV cell, the circuit is open, I = 0 and V = V_{OC} as shown in Figure 7, where V_{OC} depend on the quality of the material (typically silicon). But considering an ideal PV cell and neglecting resistances as all resistances in the system are less than zero.

$$\text{From I} = I_{Ph} - I_o[e^{\frac{V_d}{V_{th}}} - 1] - [\frac{V+IR_S}{R_{sh}}] \quad (23)$$

(c) Open Circuit Voltage (V_{oc})

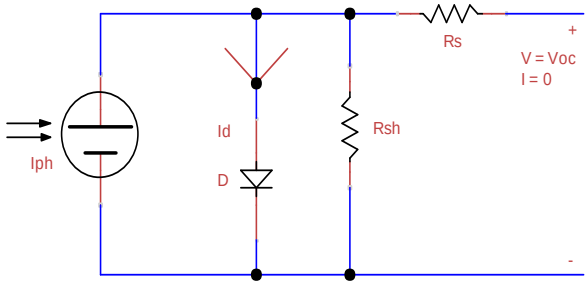

Figure 8: Equivalent circuit diagram of photovoltaic cell model showing open circuit voltage

In this case we neglect all resistances and I = 0, therefore equation 23 becomes

$$0 = I_{Ph} - I_o[e^{\frac{qV}{akT}} - 1]$$

$$\frac{I_{Ph}}{I_o} = e^{\frac{qV_{oc}}{akT}} - 1$$

Applying In (log) to both sides,

$$\ln(\frac{I_{Ph}}{I_o} + 1) = \ln(e^{\frac{qV_{oc}}{akT}})$$

$$V_{oc} = \frac{akT}{q}\ln(\frac{I_{Ph}}{I_o} + 1)$$

It can be seen that I_o is a component of temperature, as such V_{oc} is a strong function of temperature dependence with a high negative temperature coefficient. However, this is not the too good to be modeled because of temperature dependence, hence short circuit current will be considered.

(d) Short Circuit Current (I_{sc})

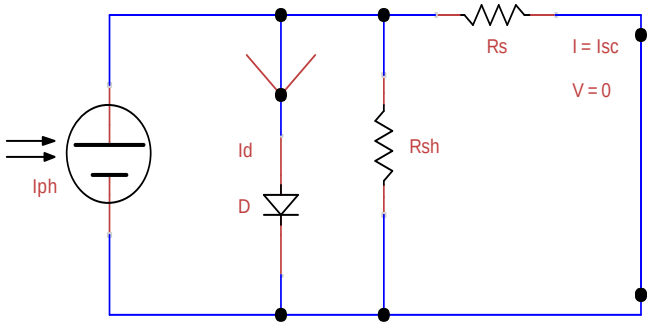

Figure 9: Equivalent Circuit Diagram of Photovoltaic Cell Model with Output short

In this case, with small value of R_s compared to zero (i.e R_s = 0), the maximum possible current from the PV cell can be calculated as follows;

From (Bana and Saini, 2016), we have that; $I = I_{Ph} - I_o[e^{\frac{V_{oc}}{V_{th}}} - 1] - [\frac{V+IR_S}{R_{sh}}]$

For open circuit; I = I_{sc} and V_{oc} = 0

$$I_{sc} = I_{ph} \quad (24)$$

It is also observed that, the photon generated current which is equal to I_{sc} and it is directly proportional to the irradiance, the intensity of illumination, to PV cell (Adel El, 2010). That is, as the incident angle changes, so does the maximum photo current of PV cell. The change can be calculated using Equation (25) below.

$$I_{ph} = I_{max}\text{Cos }\theta \quad (25)$$

In this case, two model assumption based on the solar intensity source are considered;

Assumption 1: Varies (changes) and photovoltaic cell is static, Equation 25 holds.

Assumption 2: varies (changes) with respect to the photovoltaic cell, Equation 25 becomes

$I_{sc} = I_{max}\,\text{Sine}\,\theta$. But since the goal is to maintain the orthogonality of the solar incident with respect to the solar panel, Equation (24) is substituted into (25) then,

$$I_{sc} = I_{max}\text{Sine }\theta \quad (26)$$

$$\frac{I_{sc}}{Sine\,\theta} = I_{max}$$

Where; $I_{max} = I_{ph}$ = Maximum photon current (eV)

I_{sc} = I = Output current of the PV cell (Ampere)

Therefore, the actual output equation becomes

$$\text{I} = I_{ph}\text{Sine }\theta \quad (27)$$

The transfer function of the PV cell becomes;

$$\text{T.F} = \frac{I}{Sine\,\theta} = I_{ph} \quad (28)$$

Equation 28 is that transfer function of the photovoltaic cell (solar panel) of the system.

(v) Modeling of the Close Loop Transfer Function of the Cascade Control System

$$\text{Lets } K_1(s) = T.F_{PI} = \frac{R_2(s)}{E_v(s)} = \frac{K_D S^2 + K_p S + K_I}{S} \quad (29)$$

$$K_2(s) = T.F_{PI} = \frac{U(s)}{E_\theta(s)} = \frac{K_p S + K_I}{S} \quad (30)$$

$$M(s) = \text{T.F}_M = \frac{\theta(s)}{E(s)} = \frac{K}{S[(R_a+SL_a)(J_s+\text{b}) + KK_b]} \quad (31)$$

$$P(s) = \text{T.F}_P = I_{ph} \quad (32)$$

To evaluate the transfer function of the system, we first consider the transfer function of the inner loop, we use the inspection approach (Anonymous, 2012)

$$\text{T.F} = \frac{Forward\ Loop}{1+Loop\ Transfer\ Function}$$

$$T.F_{Inner\ Loop}\ \frac{\theta(s)}{r_2(s)} = \frac{K_2(s)M(s)}{1+K_2(s)M(s)} \quad (33)$$

By inspection and using the formula in Equation (35) it becomes,

$$T.F_S = \frac{I(s)}{r_1(s)} = \frac{K_1(s)[\frac{K_2(s)M(s)}{1+K_2(s)M(s)}]P(s)}{1+\frac{K_1(s)K_2(s)M(s)\ \ P(s)}{1+K_2(s)M(s)}}$$

Multiplying $1 + K_2(s)M(s)$ by both the numerator and denominator we arrived at;

$$\boldsymbol{T.F_S = \frac{I(s)}{r_1(s)} = \frac{K_1(s)K_2(s)P(s)}{1+K_2(s)M(s)\ \ + K_1(s)K_2(s)M(s)\ \ P(s)}} \quad (34)$$

But the output Equation becomes;

$$I(s) = (\frac{K_1(s)K_2(s)P(s)}{1+K_2(s)M(s)\ \ + K_1(s)K_2(s)M(s)\ \ P(s)})r_1(s) \quad (35)$$

Substituting Equation (29), (30), (31) and (32) into (35), it becomes;

$$\frac{\text{I(s)}}{\text{r}_1\text{(s)}} = \frac{\left(\frac{K_D S^2+K_P S+K_I}{S}\right)\left(\frac{K_P S+K_I}{S}\right)(I_{ph})}{1+\left(\frac{K_P S+K_I}{S}\right)\left(\frac{K}{S[(R_a+SL_a)(J_a+b)+KK_b]}\right)+[(\frac{K_D S^2+K_P S+K_I}{S})(\frac{K_P S+K_I}{S})(\frac{K}{S[(R_a+SL_a)(JS+KK_b]})(I_{ph})]} \quad \textbf{(36)}$$

Resolving Equation (35) appropriately by simplification, it then becomes;

$$\frac{\text{I(s)}}{\text{r}_1\text{(s)}} = \frac{I_{ph}(K_D K_p S^3+K_D K_I S^2+K_p^2 S^2+2K_p K_I S+K_I^2)[(R_a+Sla)(Js+b)+KK_b]S}{S^3[(R_a+Sla)(Js+KK_b)]+S(K_p S+K_I)K+I_{ph}(K_D K_p S^3+K_D K_I S^2+K_p^2 S^2+2K_p K_I S+K_I)} \quad \textbf{(37)}$$

Equation (37) becomes the general close loop transfer function of the cascade control system.

(vi) Open Loop Transfer function of the Main Process Plant

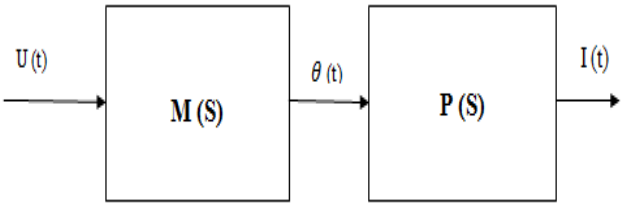

Figure 10: Block Diagram of Open Loop of the Main Process System

The equation of the feedback path of Figure 1.0 produced;

$$\text{I(t)} = \text{P(s)} \times \theta\ \text{(t)} \quad (38)$$

$$\theta\ \text{(t)} = \text{M(s)} \times \text{U (t)} \quad (39)$$

Applying Laplace transform to Equation (38) and (39), they become;

$$\text{I (s)} = \text{P(s)} \times \theta\ \text{(s)} \quad (40)$$

$$\theta\ \text{(s)} = \text{M(s)} \times \text{U (s)} \quad (41)$$

Substituting Equation (41) into (40) produces;

$$\text{I (s)} = \text{P(s)} \times \text{M(s)} \times \text{U (s)}$$

But by rearrangement we have;

$$\frac{I\ (s)}{U(s)} = \text{P(s)} \times \text{(M(s)} \quad (42)$$

Substituting Equation (31) and (32) into (33) we have;

$$\frac{I\ (s)}{U(s)} = (I_{ph})(\frac{K}{S[(R_a+SL_a)(J_s+\text{b}) + KK_b]})$$

Therefore, the open loop Transfer Function of the process becomes,

$$\frac{I\ (s)}{U(s)} = \frac{I_{ph}K}{S[(R_a+SL_a)(J_s+\text{b}) + KK_b]} \quad (43)$$

(vii) System Simulink Models and Simulation

This is the area where all the sub-system and main system simulink are built based on the developed mathematical models via MATLAB software. In other words, all the system mathematical transfer functions are used to construct simulink block for possible simulation as well as obtaining step and frequency response. The step and frequency response is based on the open and closed loop response.

(a) Open Loop Method (Step Response)

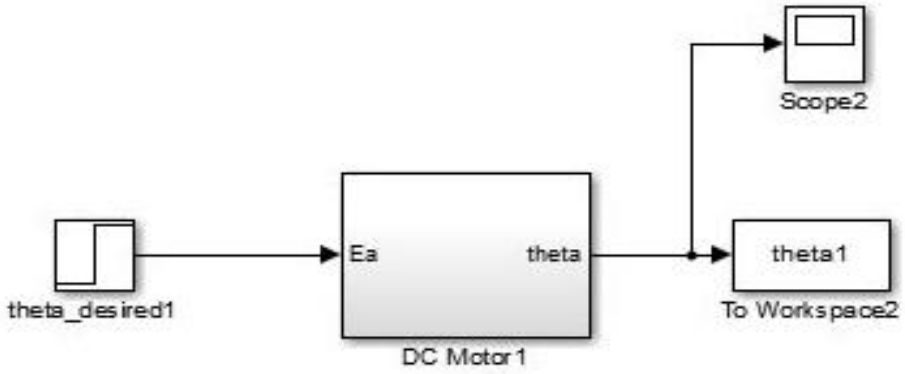

Figure 11: Simulink model of dc motor system

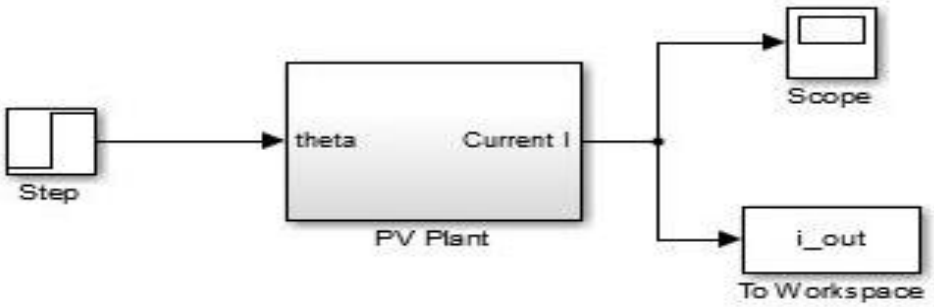

Figure 12: System simulink model of photovoltaic

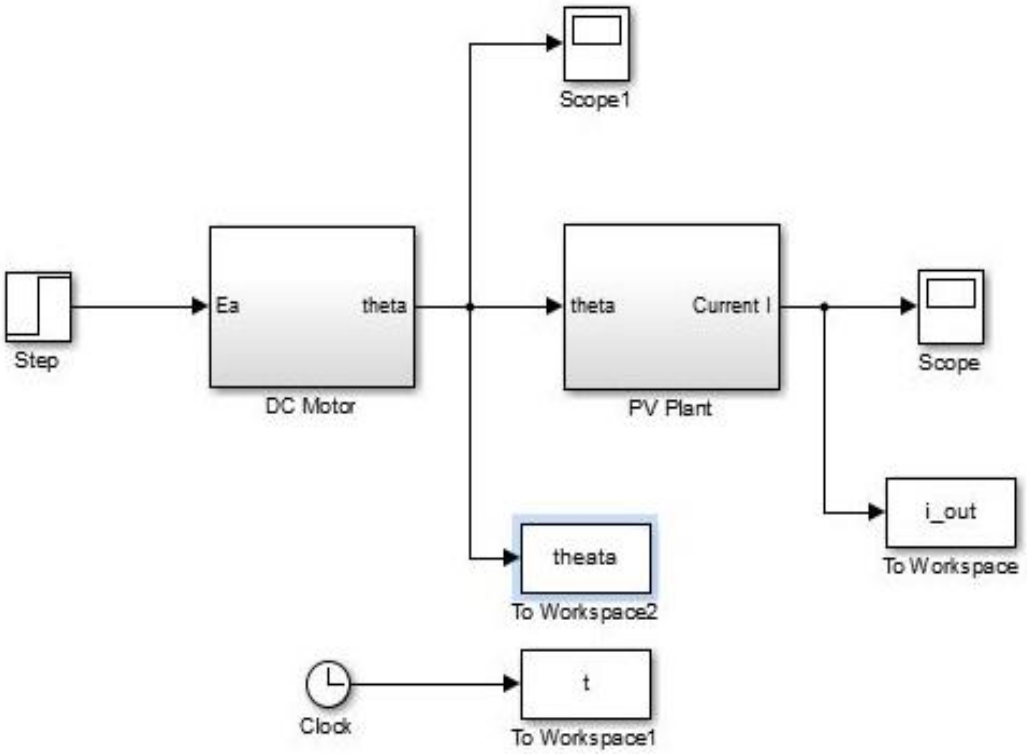

Figure 13: Simulink diagram of open loop process plant

(b) Closed loop method (Frequency Response)

Table 1.0: Zeigler Nichols Tuning Table

Controller type	Kp	Ki	Kd
P	0.5Ku		
PI	0.45Ku	0.54ku/Tu	
PID	0.6KU	1.5Ku/Tu	0.6Ku/Tu

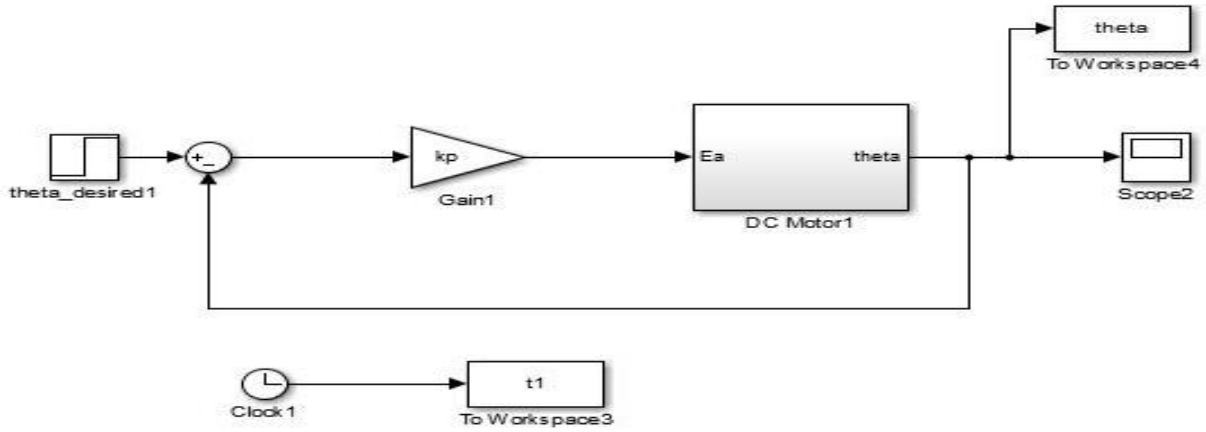

Figure 14: Simulink model of Kp on dc motor system

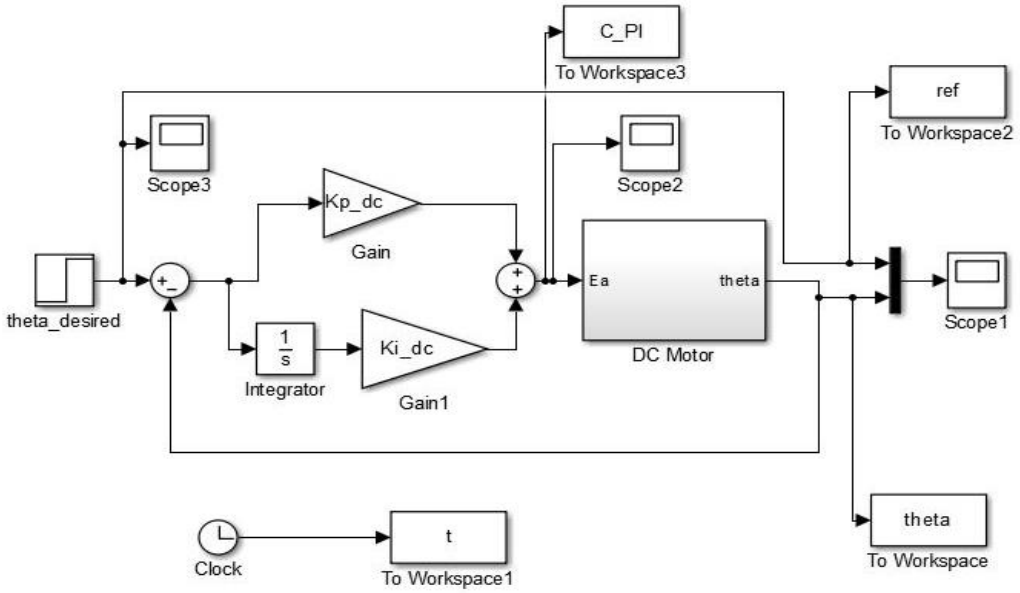

Figure 15: Closed loop Simulink model of dc motor with controller

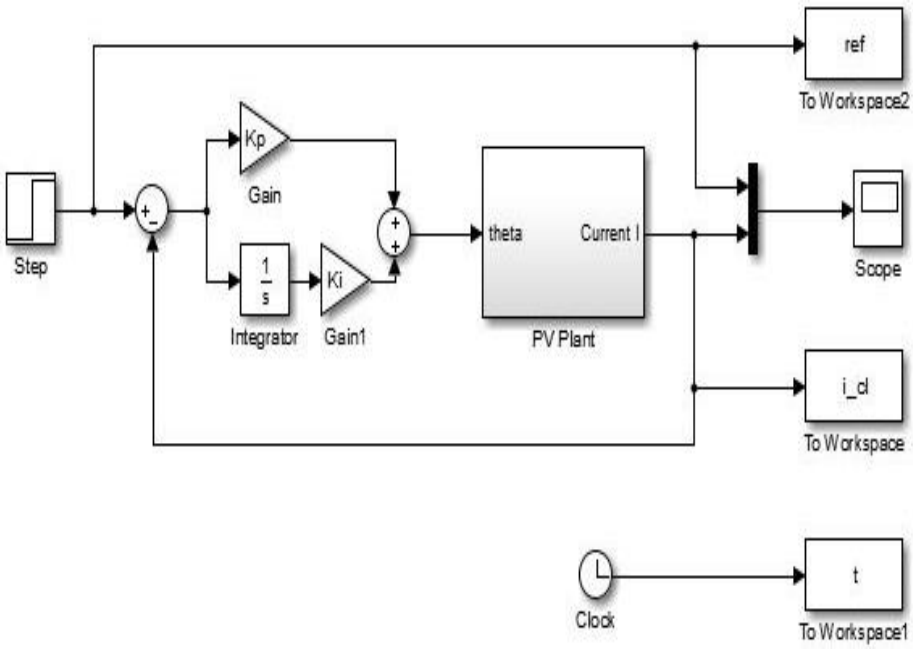

Figure 16: Closed loop Simulink model of PV with PI controller

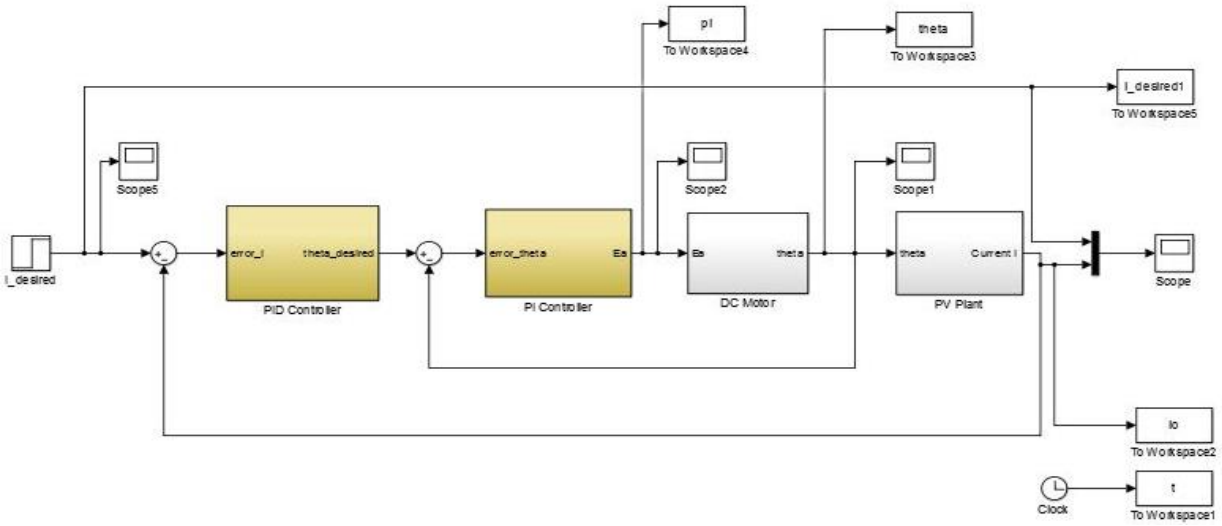

Figure 17: Closed loop Simulink model of cascade control system of the solar tracker

(vii) System Performance

In the existing performance (Ep) which used internal model control (IMC-PID) controller, showed that the system rise and settling time are 1.8 second and 5.5 seconds (Bamigboye *et al.* 2016). Also, the results summarized in Table 2, shows that our new performance (Np) for rise and settling time are 0.4 second and 1.8 second respectively. Therefore, to determine our system performance over the existing systems, we have that,

$$\text{Decrease in \% in rise time} = \frac{Existing\ performance\ (Ep) - New\ performance(Np)}{Existing\ performance(Ep)} \times \frac{100}{1} \quad (44)$$

$$\text{Decrease in \% in rise time} = \frac{1.8-0.4}{1.8} \times 100 = 77.8\%$$

$$\text{Decrease in \% in settling time} = \frac{5.5-1.8}{5.5} \times 100 = 67.2\%$$

IV RESULTS AND DISCUSSIONS

Figure 18 to 27 are graphical results obtained from the Mat Lab software used in the simulation of system models. The graphical displayed in Figure (1.17 to 1.26) shows different signal and frequency response of subsystems and systems models.

Figure 18 is a step response of an open loop dc motor system. The step response is obtained from a Simulink block model, when a step input is applied into the input of the dc motor and a corresponding response is obtained across the output of the dc motor. However, it is a graph where the angle of the dc motor (radian) is plotted against

time (second). The plot shows a straight line graph where the signal passes through the origin (0, 0). The graph reveals that the dc motor angle is directly proportional to the time. In other words, the output signal continues to increase with increase in time. The system has no overshoot, no offset point, no settling time and no dead time (delay time). It all means that the speed of the dc motor keeps increases with no sign of steady state. In this case, the dc motor parameters such as speed and torque are not controlled due to the absent of feedback system, and these leads to a continuous increase in speed and torque over time (Yadav, Kamodia and Kumari, 2014). This means that when a certain step input is applied to the dc motor, the speed and torque of rotation and torque is increases moderately with respect to time but without any control in both speed and torque.

Based on the summary result in Table 3, the rise time of open loop dc motor system increases with no settling time, which means that when voltage is applied to the dc motor, the speed and torque becomes unstable as well as the system temperature (Bharathi and Kumar, 2012).Therefore, since the temperature of the system is unstable, hence it can lead to dc motor damage any short possible time (Bharathi and Kumar, 2012). Basically, since this research work is characterized by tracking solar radiation at set point, an open loop system does not match this application because in open loop, it involve a continuous spinning and rotation of dc motor shaft without any set (angle). Therefore using an open loop dc motor system in this work is not to the interest of this research work.

(i) Open Loop Step Response of the Photovoltaic (PV) System

The graph showed in Figure 19 is step response obtained from an open loop Simulink block diagram of photovoltaic system in Figure 12. The response is gotten when a step input signal is applied to the photovoltaic system and the corresponding output signal called a stem response is obtained. In other words, it is a graph of current (amperes) is plotted against time (second). The simulated result showed that the current produced by the photovoltaic cell remains constant at 841.5A throughout the time. It also revealed that the output component of the photovoltaic system is independent of time but varies with solar radiation (Dincer and Meral, 2010). In the plot, showed that the difference between the initial and final current 1.5A. This result is a simulated result and is an ordinary picture of the photovoltaic cell producing a relatively low current when the angle is not varied in accordance with the solar radiation. Therefore, this static positioning of the photovoltaic system affects the output component of the photovoltaic cell and it agrees with (Ajao *et al.,* 2013; Shareef, 2017). However, the summary result of an open loop photovoltaic system in Figure 18 has shown that the system has low performance and so it is not considered in the research work.

(ii) Open Loop step response of dc motor in cascaded system

Figure 20 shows a step response of a dc motor in an open loop cascaded system. The output signal is obtained when the dc motor output is coupled to the input of the photovoltaic system as shown in Figure 13. An oscilloscope is connected to the output of the dc motor such that the response of the dc motor in the open loop cascade system is obtained. it is also a graph of angle (radian) against time (second). This response or plot reveals the behavior of dc motor in an open loop cascaded mode. The response of the dc motor cascaded system is similar to Figure 18 when is not in the cascaded. It still shows a straight line graph passing through the origin (0, 0), where the angle is directly proportional to the time. In other words, the dc motor speed and torque increases with time, which means that in an open loop cascade, the dc motor system speed starts rotating from initial, which is from 0^0 to infinite position even with no accuracy. This is so because there is no feedback path which could control both speed and torque and make the system stable and accurate (Rooholahi and Reddy, 2015). Therefore, Table 3 has summarized that the open loop cascade system shows that there is no settling time, no stable point and no steady state. Therefore, since there is a very high level of instability and inaccuracy in the cascade system, meaning that coupling a dc motor without a feedback path is not ideal in this case and as such it cannot be applied in this design.

(iii) Closed Loop Frequency response of dc motor for proportional gain (Kp)

Figure 22 to 23 show the frequency response of a closed loop dc motor system with a proportional gain (Kp). The results are obtained from Figure 14, where a proportional controller is used to tune the dc motor to a stable state. In this case, a step input is applied through the summer input and proportional term so as to provide the required voltage to the dc motor input and the corresponding response is obtained at the output. The response obtained at the dc motor output is an undamped oscillation response with equal amplitude. Figure 22 is an amplified response of Figure 23, where the amplitude of the response is so adjusted so that correct readings in terms of ultimate gain (Ku) as well as ultimate period (Tu) is seen and taken clearly. The ultimate period (Ku) of the closed loop dc motor using proportional controller is 0.5, while the ultimate gain (Tu) at indefinite steady state oscillation is 20,022. This values agree with other studies that the higher the value of ultimate gain (Tu), the faster, smoother, more stable and accurate the system becomes (Kumar, 3013).

(iv) Closed Loop frequency Response of dc motor System

The plot in Figure 24 is the frequency response of closed loop dc motor. This response is obtained when the Simulink block model in Figure 15 is simulated. It is also a simulated result of angle against time. The plot revealed the action of proportional and integral term effect on the dc motor system with a feedback path. The graph also revealed a closed loop characteristics of dc motor in terms of signal rise time, settling time, overshoot, steady state error which are interpreted into dc motor speed, torque, positioning, accuracy and temperature.

In the simulated result, the signal rises from 0 and the frequency response signal rise time was 0.5 second, while the settling time was 1.6 seconds (see Table 4). It

shows that the rise and settling time is relatively moderate as it agrees with other findings and studies (Bamigboge *et al*., 2016). The plot also shows clearly that there is no overshoot and offset in the system which is a good response from any good proportional and integral controlled system (Rao, 2013); (Loucif, 2016). It means that the present of proportional and integral term acted on the overshoot and offset components, hence propagate and eliminate it completely as it is summarized in Table 4. The system portrays an automatic solar tracking system, whereby in real time or in practice, it reveals the behavior of the dc motor in terms of speed in rad/secs. It shows that as the dc motor speed increases rapidly when voltage is applied, the proportional and integral (PI) slave controller (inner loop controller) adjust in other to reduce the error between the desired and actual speed of the dc motor system which agrees with (Dubey, 2013). Also, it takes 0.5 seconds for dc motor to change its angle or turns and then stabilizes at 1.6 seconds when a certain small voltage is applied. This implies that a small voltage applied to the dc motor will cause it to respond faster and at a moderate speed and torque.

(v) Closed Loop Frequency Response of Photovoltaic Cell (PV) System

The graph in Figure 25 is the closed loop frequency response of a photovoltaic cell with proportional and integral (PI) controller. It is a plot of output current (ampere) against time (secs). The plot is obtained when the Simulink model in Figure 16 was simulated. It revealed the behavior of proportional and integral term action on photovoltaic cell positioning. The frequency response curve shows a relative longer time for the signal to settle at set point (100A) as compared to that of the closed loop frequency response in Figure 24. According to the response curve, it took 1.6 second for the signal to rise from it initial point before getting to the settling point, that the rise time. The response also reveals that it took 5.5 seconds for the signal to get settled (settling time). It shows that there is a small delay in the process as it took 1.6 second for the signal to rise as also shown in Table 4. This implies that the speed is reduced due to the applied load and torque is increased.

However, in practice the curve means that during closed loop frequency response of the photovoltaic cell, it output current (I_o) increases and decreases steadily with respect to increase or decrease in solar radiation, and proportional integral master controller (outer controller) scales and reduces the error between the desired and actual output. This is called the desired or set point which is the desired angle (i.e right angle), meaning that the proportional integral controller tilts and set the solar panel such that it would always maintain an angle perpendicular to the solar angle (i.e 90^0) to produce optimum output current (I_o) which agrees with (Ajao *et al.*, 2013; Mohammed *et al.*, 2014).

(vi) Time response of the dc motor in cascade system.

Figure 21 is the time response of dc motor in the cascade system. It is also the response of angle (radian) against time (second). The signal is gotten from the cascaded control block diagram system, which is the Simulink block in Figure 17. The signal is also obtained when an oscilloscope is connected to the output of the dc motor with respect to time. The output signal revealed the behavior of dc motor in a cascaded control system, especially when it output is coupled to the load (solar panel). The dc motor behavior includes the delay time, speed, rise time and torque. The simulated time response result shows that it took about 40.4 seconds delay time for the dc motor to response to the applied input. The graph also reveals that the dc motor has a moderate speed as the signal rise time increases sharply with a moderate torque. In practice, implies that in the cascade control system, it took some time for the dc motor to start rotating when an input voltage is applied. The time taken for the dc motor to rotate is relatively long but since this is just a simulated result the real time is usually shorter. The graph of time response also revealed that the dc motor rotates with moderate speed and torque as it covers a wider angle within few seconds. This also implies that the dc motor with moderate speed and torque is capable of tilting the load (photovoltaic cell) to a set point irrespective of the difference in angle.

(vii) Closed Loop Frequency Response of a cascaded control system (Solar Tracker)

Figure 27 is the closed loop frequency response of a cascaded control system. It is also known as the closed loop response of the overall system, called solar tracker. It is the output response gotten from the Simulink block diagram of Figure 17. That is, the signal is obtained when a step input is applied into the summer junction of the outer proportional controller and the output frequency response is taken from the photovoltaic cell output. The frequency response revealed the overall system behavior especially when all the components are working. The graph shows the rate and possibility of working, including the system stability, accuracy, response time, speed, torque.

According to the overall frequency response, the output response oscillates with some level and degree of spikes. In other words, the output response is a time invariant since it contains some transient components. The signal also spans between the bandwidth of ± 1000 A (i.e +1000 and -1000). This implies that the system is relatively stable and accurate in term of angle and positioning of load (solar panel). It also means that, the system is capable of demonstrating high level of tolerance in terms of torque, disturbance rejection and speed. That is the system through the present of the proportional integral (PI) controllers (inner and masters) is capable of adjusting between the slow and moderate speed when coupled with solar panel. The present of spike in the response is due to the fact that the final output component that is, the output current (I_o) is independent of time but dependent of photo current (i.e solar irradiance) (Chikate and Sadawarte, 2015).

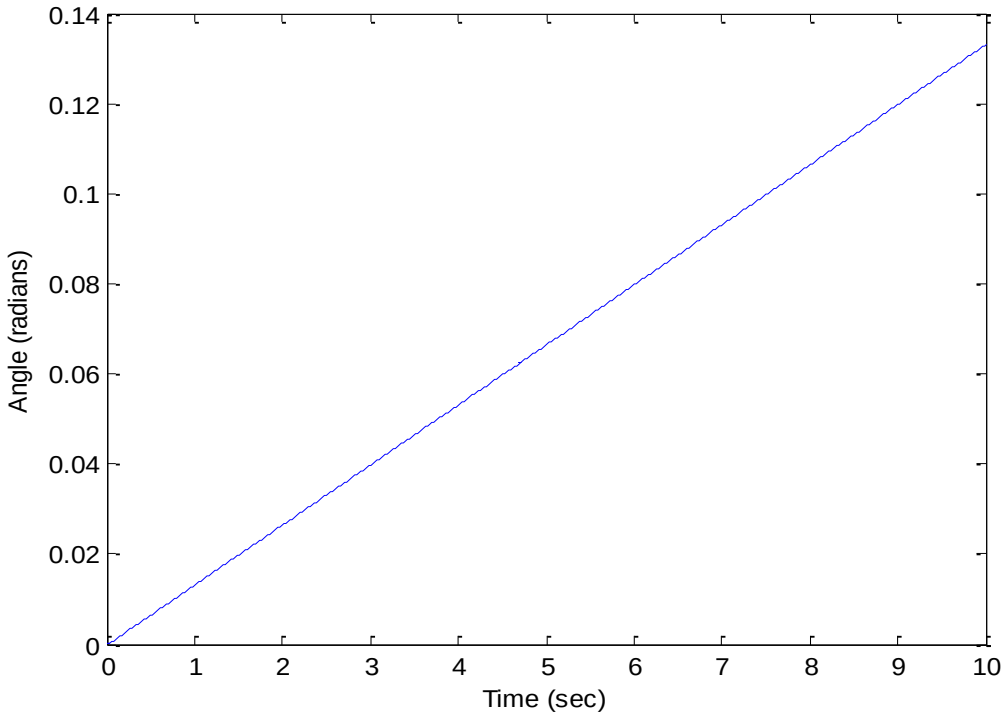

Figure 18: Open loop step response of dc motor

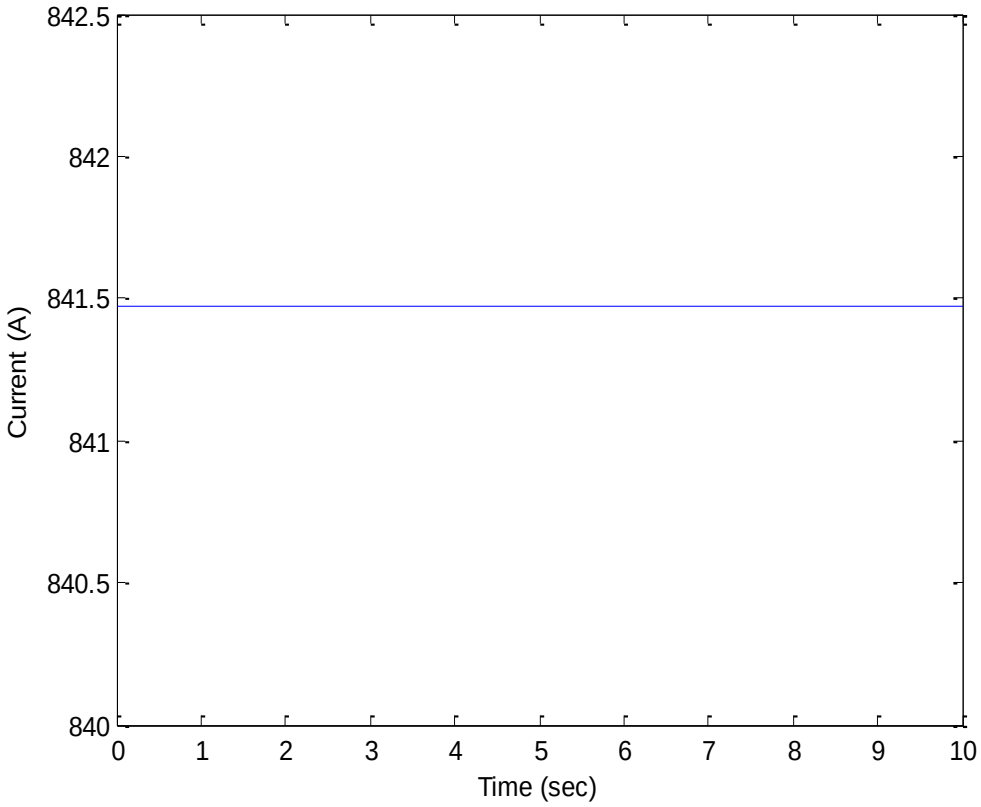

Figure 19: Open loop step response of photovoltaic cell (PV)

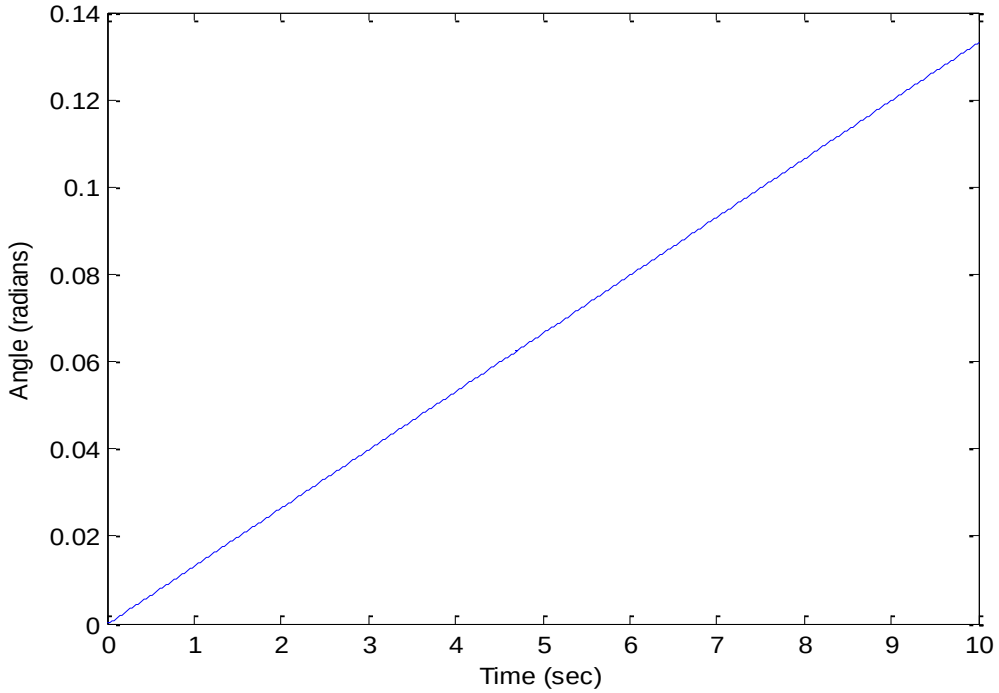

Figure 20: Open loop step response of dc motor coupled to PV system

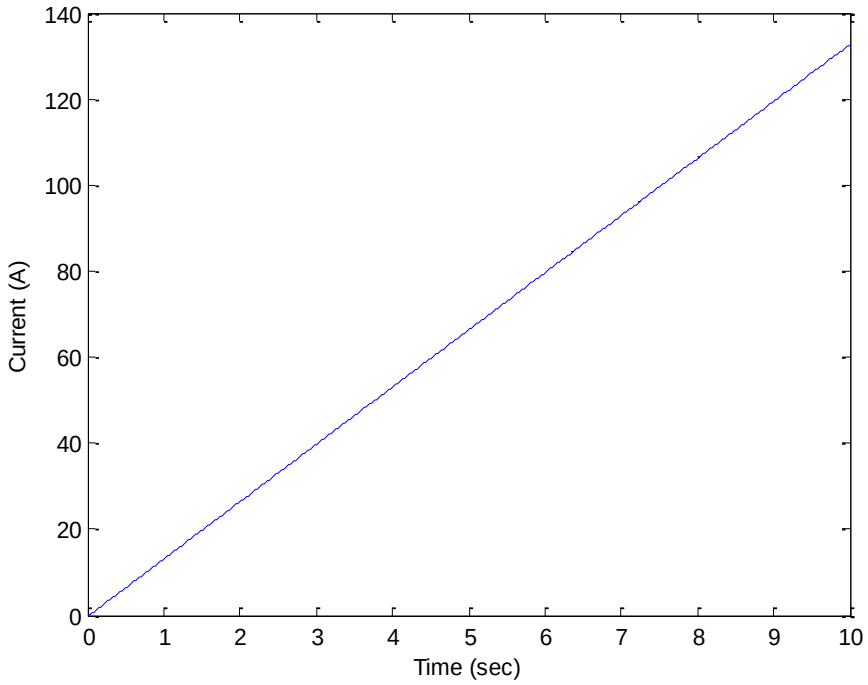

Figure 21: Open loop step response of the process plant

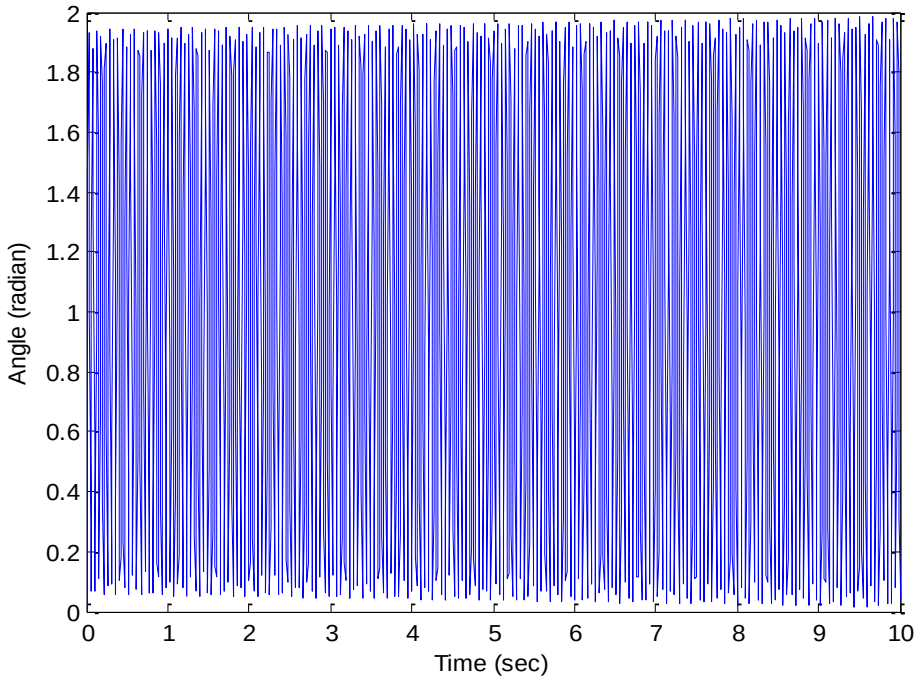

Figure 22: Frequency response of kp controller on dc motor

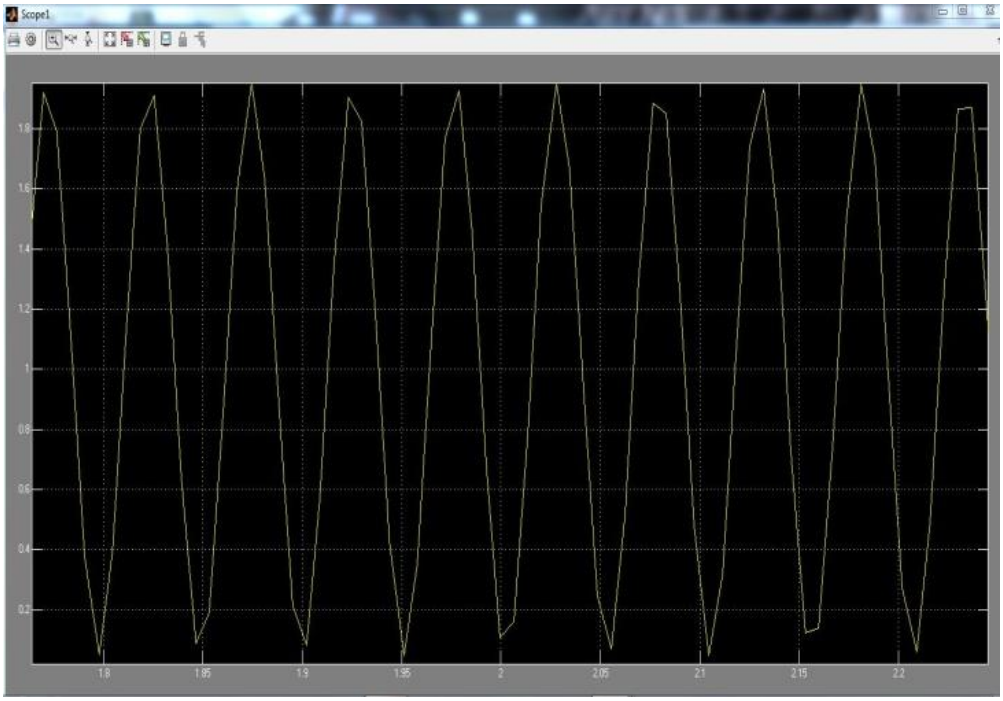

Figure 23: Frequency response of kp controller on dc motor (zoom)

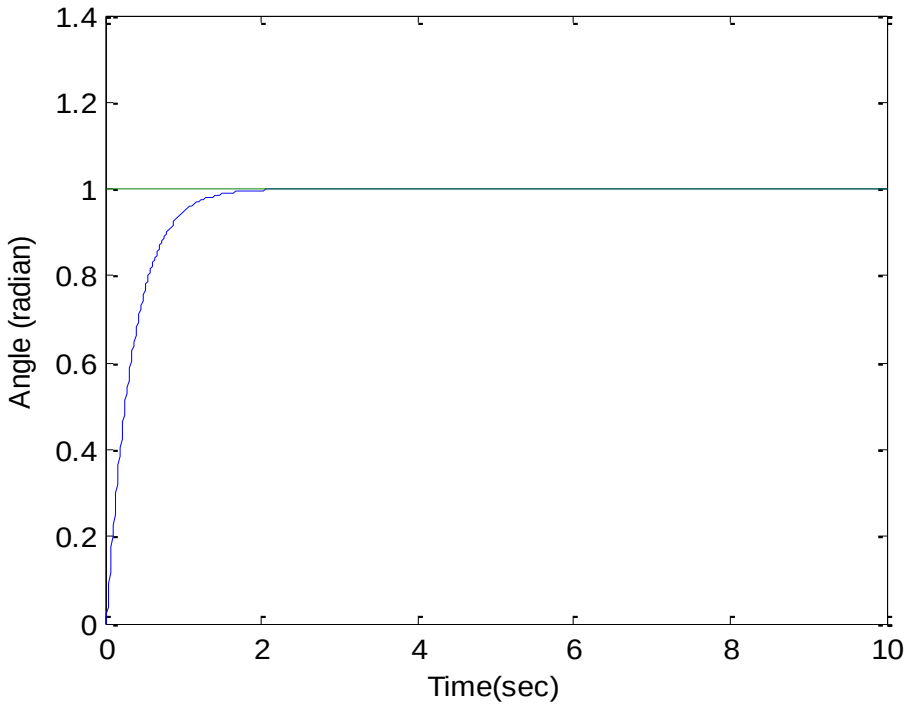

Figure 24: Output closed loop response of dc motor with controller

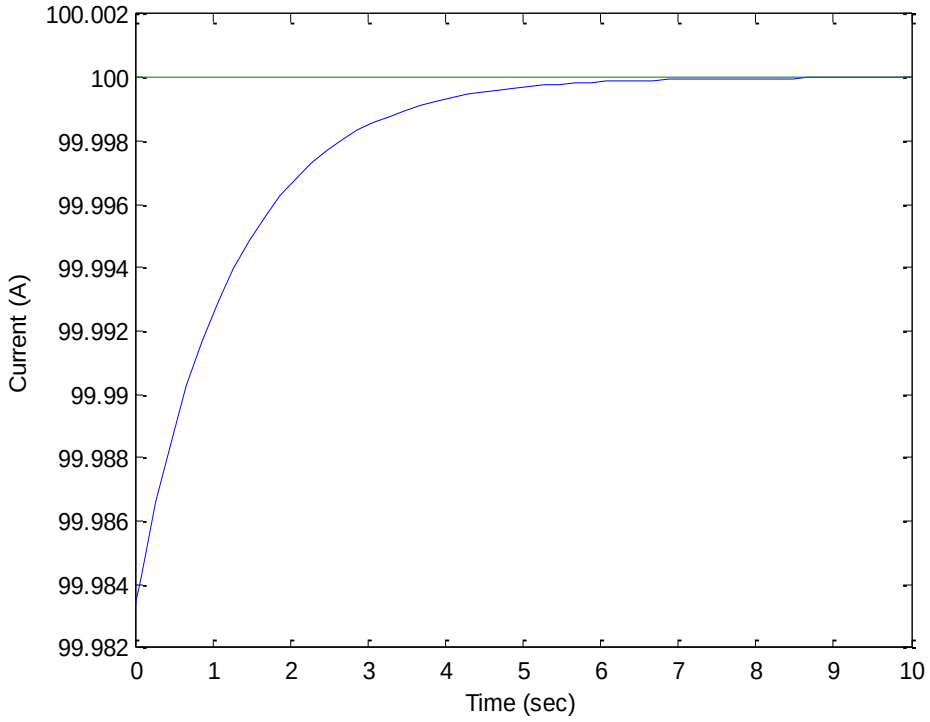

Figure 25: Closed loop frequency response of PV system with PI controller

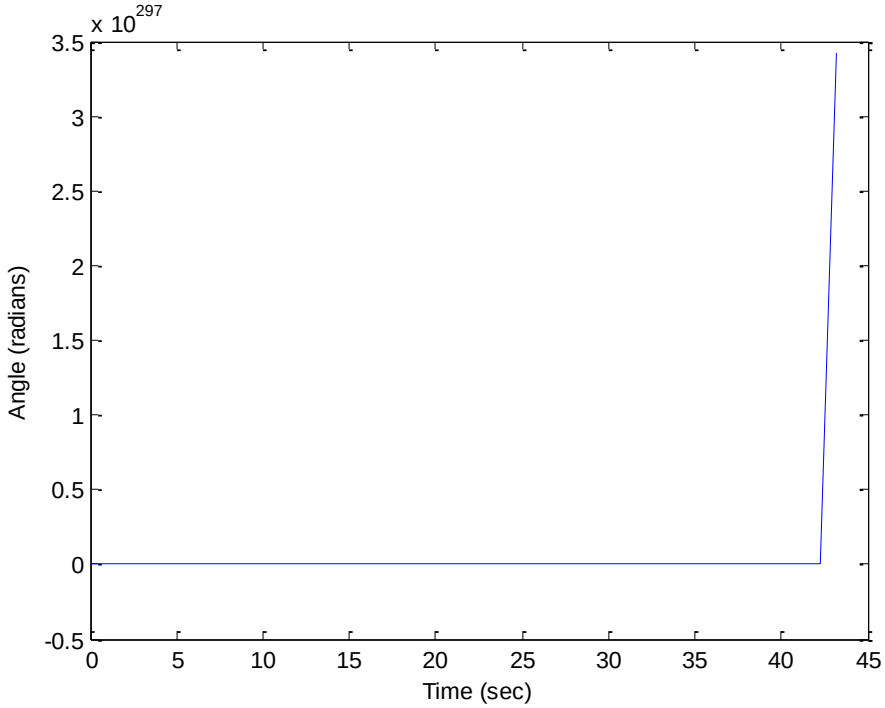

Figure 26: Time response of dc motor in cascaded system

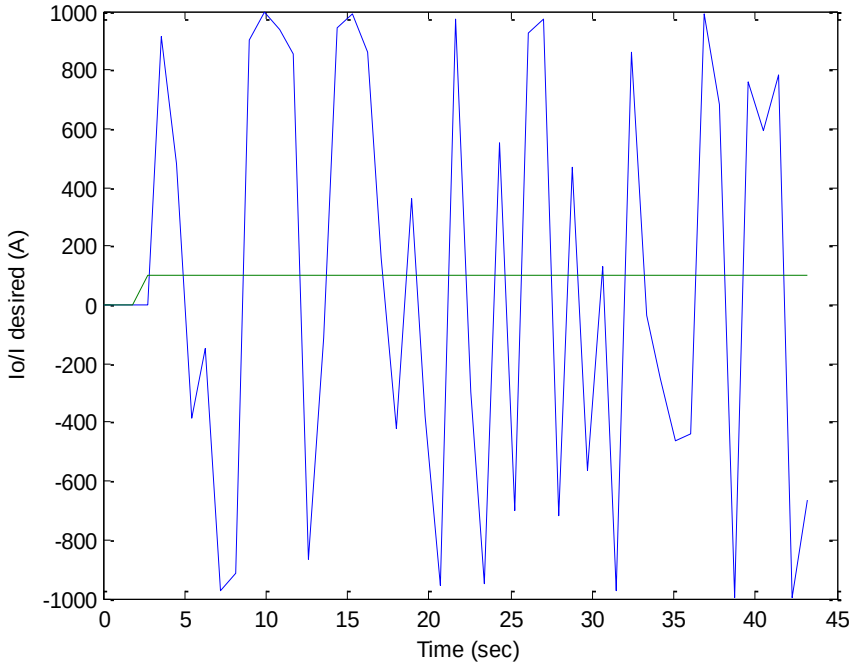

Figure 27: Frequency response of cascade control system

Table 3: Summary of Open Loop Response (Step Response)

Type of System	Rise Time (sec)	Steady State Error	Settling Time (sec)	Time Delay (sec)
DC motor	Not defined	Not defined	0	0
PV cell	Constant	Not defined	0	0
Cascade	Not defined	Not defined	0	0

Table 4: Summary of Closed Loop Response (Frequency Response)

Type of System	Rise Time (sec)	Steady State Error	Settling Time (sec)	Time Delay (sec)	Overshoot	Undershoot
DC motor	0.4	0	1.8	0	0	0
PV cell	1.6	0	5.5	0	0	0
Cascade	Stable	Stable	Not applied	Not applied	Not applied	Not applied

VI CONCLUSION

Modeling, characterization and optimization of solar tracker using proportional integral controller has been achieved. Basic mathematical models have been successfully formulated, built and developed. These mathematical models include transfer function for both inner and outer loop of proportional integral controllers (Master and slave proportional controllers), electrical component of the dc motor, mechanical component of the dc motor, transfer function of the dc motor, input and output component of the photovoltaic cell; that is diode equation, series resistance open circuit voltage equation, short circuit equation and shunt resistance equation. Also, Simulink models of the various sub-systems and the overall cascade control system have been designed and developed using MATLAB software. The sub-systems include; proportional controller transfer function, electrical and mechanical components of the dc motor transfer function, photovoltaic cell transfer function and the overall system transfer function. Also, simulation of subsystems models has been carried out with different time and frequency responses fantastically obtained. The results obtained shows that the subsystem and system models have worked as anticipated. The experimental simulation results of various subsystems of proportional integral controller with dc motor, proportional integral controller with photovoltaic cell and overall cascade control system time responses which showed a reduced percentage system rise time by 77.8%, settling time by 67.2%. The responses also showed no overshoot but eliminated steady state error. It is seen that the use of proportional controllers in solar tracking system has improved the tracking stability characteristics in terms of desired speed, positioning, tolerance, time and frequency response. However, it is therefore recommended that further research should also be carried out on the methods of cooling and maintaining photovoltaic cell temperature as well as advance controllers, as it will boast solar panel efficiency.

REFERENCES

Adel, E. S. (2010). PV Cell Module Modeling & ANN Simulation for Smart Grid Applications. *Journal of Theoretical and Applied Information Tech.*

Ajao, K. R., Ambali, R. M. and Mahmoud, M. O. (2013). Determination of the Optimal Tilt Angle for Solar Photovoltaic Panel in Ilorin, Nigeria. *Journal of Engineering Science and Technology Review*, 6(1): 87-90.

Anonymous (2012). Transfer Function Models of Dynamical Processes. www.chemeng.queensu.ca/courses/CHEE319/documents/CHEE319_notes_2012_lecture4.pdf. Retrieved on 3rd September 2018.

Bala, K. and Rajesh S. (2014). MPPT Controller Based Solar Tracking System. *International Organisation of scientific Research in Journal of Mechinical and Civil Engineering*, 78 – 83

Balabel, A., Mahfouz, A. A. and Salem, F. A. (2013). Design and Performance of Solar Tracking Photo-Voltaic System; Research and Education. *International journal of control, automation and system,* 1(2): 49–55.

Bamigboye O., Oladayo and Adewunmi O. T. (2016). Development of Solar Tracking System Using Imc-Pid Controller. *American Journal of Engineering Research*, 5(5): (1-8).

Bamigboye O., Oladayo and Adewunmi O. T. (2016). Development of Solar Tracking System Using Imc-Pid Controller. *American Journal of Engineering Research*, 5(5): (1-8).

Bana, S. and Saini, (2016). A mathematical modeling framework to evaluate the performance of single diode and double diode based SPV systems. *ScienceDirect*. 2, 171-187.

Baranwal, A. and A. Dwived, A (2014). Optimization of solar energy using solar tracking system.

National Conference on Futuristics in Mechanical Engineering. Available at: www.researchgate.net/profile/abhishek_dwivedi12. Retrieved on 12th January 2018

Bharathi, M. and Kumar, G. (2012). Design approach for pitch axis stabilization of 3-dof helicopter system an lqr controller. *International Journal of Advanced Research in Electrical, Electronics and Instrumentation Engineering*, 1(5): 351-365.

Chikate, B. V and Sadawarte, Y. A. (2015). The Factors affecting the performance of solar cell. *International Conference on Quality Up-gradation in Engineering, Science and Technology*, 1 – 5.

Deb, G. and Roy, A. B. (2012). Use of solar tracking system for extracting solar energy. *International Journal of Computer and Electrical Engineering*, 4(1): 42–46.

Dincer, F. and meral, M. E. (2010). Contrical factor that affecting efficiency of solar cells. *Smart Grid and Renewable Energy Scientific Research* 1: (47 - 50).

Dubey, S. and Srivastava, S. K. (2013). A PID controlled real time analysis of dc motor. *International Journal of Innovative Research in Computer and Communication Engineering,* 1(8): 1965-1973.

Islam, M. A., Hasanuzzaman, M., Rahim, N. A., Nahar, A. and Hosenuzzaman, M. (2014). Global renewable energy-based electricity generation and smart grid system for energy security. The Scientific World Journal. 1 – 13.

Kalanithi, B. and Rajesh, S. (2014). MPPT Controller based solar tracking system. *Journal of Mechanical and Civil Engineering*, 78–83.

Kiyak, E. and Gol, G. (2016). A comparison of fuzzy logic and PID controller for a single-axis solar tracking system. *SpringerOpen journal*, 1 – 14.

Kumar, N. and Sharma, N. (2016). Improve performance of PV system by PID controller. *International Journal of Science, Engineering and Technology*, 4(1): 227 – 232.

Kumar, R., Sunil, K. Singla, S. K. and Vikram (2013). A Comparative Analysis of different Methods for the tuning of PID Controller. *International Journal of Electronics Communications and Electrical Engineering,* 3(2): 1 – 17.

Loucif, F. (2016). DC motor speed control using PID controller, *Research Gate*, Conference Paper. 1 – 6.

Ozerdem, O. C. and Shahin, A. (2014). A PV solar tracking system controlled by Arduino/Matlab/Simulink. *International Journal on Technical and Physical Problems of Engineering*, 6(4): 5-10.

Rao, V. M. V. (2013). Performance Analysis of speed Control of Dc motor Using P, PI, and PID controllers. *International Journal of Engineering Research & Technology*, 2(5): 60 – 67.

Rooholahi, B. and Reddy, P. L. (2015). Concept and application of PID control and implementation of continuous PID controller in Siemens PLCs. *Indian Journals of science and Technology*, 8(35): 1 – 9.

Shareef, S. J. (2017). The impact of tilt angle on photovoltaic panel output. *ZANCO Journal Of Pure and Applied Science*, 29 (5): 112 – 118.

Sparavigna, A. C. (2015). A historical discussion of angular momentum and its Euler equation. *International Journal of Sciences*. 1(07): 34 - 38.

Wendy, M Van Norden, (2009), The Sun and the water Cycle. National Aeronautics and Space administration. 6-34, www.nasa.gov. Retrieved on 21th January 2017

Yadav, M., Kanodia, K, and Kumari, N. (2014). Review paper on controlling the speed of Dc motor with high accuracy and demerits of other speed controlling techniques. *International Journal of Enhanced Research in Science Technology & Engineering*, 3(11): 73 – 77.